Clim. Past Discuss., 3, 1261–1282, 2007
www.clim-past-discuss.net/3/1261/2007/


**Climate of the Past Discussions**

*Climate of the Past Discussions* is the access reviewed discussion forum of *Climate of the Past*

# Modeling a strong East Asian summer monsoon in a globally cool Earth, the MIS-13 case

**Q. Z. Yin, A. Berger, E. Driesschaert, H. Goosse, M. F. Loutre, and M. Crucifix**

Institut d'Astronomie et de Géophysique G. Lemaître, Université catholique de Louvain, Chemin du Cyclotron 2, 1348 Louvain-la-Neuve, Belgium

Received: 5 November 2007 – Accepted: 12 November 2007 – Published: 26 November 2007

Correspondence to: Q. Z. Yin (yin@astr.ucl.ac.be)



**Abstract**

Deep-sea and ice-core records show a significant reduced amplitude of the ice volume, temperature and greenhouse gases variations before Marine Isotope Stage (MIS) 11, about 400 000 years ago, with less warm (more glaciated) interglacials and less cold glacials. At the same time, the loess in northern China, the sedimentary core in the eastern Tibetan Plateau and the palaeosols in southern China all record an unusually warm and wet climate during MIS-13 (about 500 000 years ago), indicating an extremely strong East Asian summer monsoon. To understand this seeming paradox of a strong East Asian summer monsoon occurring during the cool MIS-13, a three-dimension Earth system Model of Intermediate complexity is used. Modeling results show that this very strong MIS-13 East Asian summer monsoon, identified from the precipitation, horizontal and vertical (omega) wind, and pressure (geopotential) fields, results from the astronomical and ice sheet forcings. North Hemisphere summer at perihelion both at 529 and 506 ka BP leads to an East Asian summer monsoon stronger than during the Pre-Industrial time. In addition, the ice sheets reinforce the East Asian summer monsoon through the propagation of a perturbation wave which is induced mainly by the Eurasian ice sheet and is influenced by the Tibetan Plateau.

## 1 Introduction

Most of the $\delta^{18}$O records in deep-sea sediments show a significant reduced amplitude of the ice volume variations before Marine Isotope Stage (MIS) 11, about 400 ka ago, with less warm (cooler) interglacials and less cold glacials (Imbrie et al., 1984; Bassinot et al., 1994; Tiedemann et al., 1994; Shackleton, 2000; Lisiecki and Raymo, 2005). The deuterium temperature record in the Antarctic ice cores shows the same features (Jouzel et al., 2007). The amplitude of the variations of the greenhouse gases (GHG) concentration is also reduced before MIS-11 (Siegenthaler et al., 2005; Spahni et al., 2005). Explaining such a reduction in the amplitude of climate and GHG con-

centration variations before 400 ka BP is certainly one of the exciting challenges for the paleoclimate community over the next years. As this phenomenon is present in both deep-sea and ice cores, it is tempting to conclude that the climate oscillation had a reduced amplitude everywhere. This is not true. For example, the loess in northern China (e.g. Kukla et al., 1990; Guo et al., 2000), the sedimentary core in the eastern Tibetan Plateau (Chen et al., 1999) and the palaeosols in southern China (Yin and Guo, 2006) all record an unusually warm and wet climate during MIS-13, indicating an extremely strong East Asian Summer Monsoon (EASM). During the same interglacial, unusually strong African and Indian monsoons are recorded in the sediments of the equatorial Indian Ocean (Bassinot et al., 1994) and of the Mediterranean Sea (Rossignol-Strick et al., 1998). Other temperature and precipitation extremes are also recorded in sediment cores of the equatorial Atlantic, the Pacific, the subtropical South Atlantic Ocean (e.g. Gingele and Schmieder, 2001; Harris and Mix, 1999; Wang et al., 2004) and in the Lake Baikal of Siberia (Prokopenko et al., 2002) (for detail, see Yin and Guo, 2007).

To understand the seeming paradox of a strong EASM occurring during the relatively "cool" MIS-13, we performed simulations of the Earth climate at MIS-13, analyzing both the global climate and the more regional East Asian features related to the EASM. For meeting this goal, we will investigate the response of the LOVECLIM model to prescribed GHG concentration, astronomical and ice sheet forcings of MIS-13. Three periods of time will actually be selected: 495, 506 and 529 ka BP for which sensitivity analysis to the North American and Eurasian ice sheets will also be made. The model will be introduced in Sect. 2 and the forcings will be described in Sect. 3. Section 4 will analyze the climate response during MIS-13.1 (495 and 506 ka BP experiments) with a special emphasis on the EASM. The MIS-13.3 (529 ka BP) experiments will be discussed in Sect. 5 before drawing conclusions.



## 2 The model

The model used is LOVECLIM1.1, a slightly modified version of Driesschaert et al. (2007), a three-dimension Earth system Model of Intermediate complexity. It consists of five components representing the atmosphere (ECBilt), the ocean-sea ice (CLIO), the terrestrial biosphere (VECODE), the oceanic carbon cycle (LOCH) and the Greenland and Antarctic ice sheets (AGISM) (Driesschaert, 2007). The version used in this paper takes into account the interactions between the atmosphere (ECBilt), the ocean-sea ice (CLIO), the terrestrial biosphere (VECODE) and the impact of the ice sheets on the atmosphere through albedo and topography. ECBilt is a quasi-geostrophic atmospheric model with 3 levels and a T21 horizontal resolution (Opsteegh et al., 1998). CLIO is a primitive-equation, free-surface ocean general circulation model coupled to a thermodynamic-dynamic sea ice model (Goosse and Fichefet, 1999). Its horizontal resolution is $3^{\circ} \times 3^{\circ}$, and there are 20 levels in the ocean. VECODE is a reduced-form model of vegetation dynamics and of the terrestrial carbon cycle (Brovkin et al., 2002). It simulates the dynamics of two plant functional types (trees and grassland) at the same resolution as that of ECBilt. Previous ECBilt-CLIO-VECODE model versions have been used in a large number of climate studies (reference can be made to http://www.knmi.nl/onderzk/CKO/ecbilt-papers.html), including the last interglacial and Last Glacial Maximum (LGM) climate (e.g. Timmermann et al., 2004; Duplessy et al., 2007). The model has also taken part in several model intercomparison projects for the simulation of past climate (e.g. Braconnot et al., 2007). More information about the LOVECLIM model itself and a complete list of references is available at http://www.astr.ucl.ac.be/index.php?page=LOVECLIM%40Description. For present-day conditions, LOVECLIM simulates pretty well many features of the East Asian monsoon. The January high pressure and the July low pressure are correctly represented over East Asia, as well as the associated climate fields (temperature, precipitation and wind).

## 3 Climate forcings

According to the deep-sea $\delta^{18}$O records, MIS-13 is characterized by 3 peaks: 13.11, 13.13 and 13.3 (Imbrie et al., 1984; Bassinot et al., 1994; Tiedemann et al., 1994; Shackleton, 2000; Lisiecki and Raymo, 2005). They occur respectively at about 482, 501 and 524 ka BP with a range of uncertainty of a few thousands of years. To avoid the controversy of dating uncertainty and because our aim is to study the effects of the astronomical forcing and ice sheets on the climate of MIS-13, we choose the ice volume and the orbital forcing which are representative of peak interglacial conditions, it means the maximum summer insolation and minimum ice volume recorded during MIS-13.

In our modeling experiments, the model is forced by (i) the latitudinal and seasonal distributions of the energy received from the Sun and computed from the appropriate astronomical elements (Berger, 1978), (ii) by the GHG concentration retrieved from the Dome C ice core in Antarctica and (iii) by the ice sheets assumed to exist during this interglacial. All the climatic features of the MIS-13 simulations will be compared to the simulated Pre-Industrial (PrI) climate.

### 3.1 Astronomical and GHG forcings of MIS-13.1

In order to test the sensitivity of the climate model to the astronomical forcing, we decided to run the model for two astronomically different situations which both occurred during the climatic plateau covering MIS-13.1. We considered 506 ka BP (Northern Hemisphere (NH) summer at perihelion, $\varpi$=274.05°) (Table 1), as a forcing for MIS-13.13. The astronomical forcing which can be used for MIS-13.11 at 485 ka BP ($\varpi$=268.25°, $e$=0.03857, $\varepsilon$=23.212°) being pretty close to the one at 506 ka BP, the model was not run for this date. These dates are both a few thousands of years earlier than MIS-13.11 and MIS-13.13 which can hopefully represent the possible lag between the forcings and the response of the climate system. The other date selected is 495 ka BP when the astronomical (precession) configuration is opposite to the one at 506 ka



BP, it means NH winter occurring at perihelion ($\varpi$=97.82°).

Being given the revised time scale of EPICA in Jouzel et al. (2007) and the $CO_2$, $CH_4$ and $N_2O$ concentration given in Siegenthal et et al. (2005) and Spahni et al. (2005), it was decided to use the same GHG concentration for both the 506 and 495 ka BP MIS-13.1 experiments. This hypothesis seems acceptable because the GHG values for these two dates are not much different, and averages over that period were used (Table 1). Taking the same values for the whole MIS-13.1 makes it easier also to test the sensitivity of the climate model to the astronomical forcing alone, in particular to precession.

### 3.2 North American (NA) and Eurasian (EA) ice sheets at MIS-13.1

$\delta^{18}$O of deep-sea cores show clearly that there must be ice sheets in North America and in Eurasia during MIS-13.1. Their reconstruction is unfortunately not available. Their area and volume will therefore be estimated by extrapolating the information available from their LGM reconstruction using $\delta^{18}$O – ice volume – sea level generic relationships. The Greenland and Antarctica ice sheets were kept the same as for the present-day in all the simulations. We hypothesize that the LGM total ice volume for both NA and EA was $39\times10^6$ km$^3$, a mid-range value estimated from Hughes et al. (1981), Peltier (1994, 1998, 2004), Clark and Mix (2002), Lambeck et al. (2002), and Bintanja et al. (2005). This value is actually pretty close to the ICE-4G Peltier LGM reconstruction ($36.1\times10^6$ km$^3$) and to his ICE-5G (Peltier, 2004). Using a ratio between the excess over today of ice at the LGM and at MIS-13.1 equal to that of the $\delta^{18}$O taken from Imbrie et al. (1984) (a hypothesis that we refer to as the proportionality rule) leads to about $11\times10^6$ km$^3$ of ice at MIS-13.1 for NA and EA taken together. Estimation of the volume ratio between NA and EA is less obvious. We can either assume that it was the same as at LGM (NA is twice EA in the LGM scenario) or follow Bintanja et al. (2005)'s reconstruction (EA is twice NA in the Bintanja scenario). This leads to an ice volume of 7.3 and $3.7\times10^6$ km$^3$ for respectively NA and EA in the LGM scenario or to 3.7 and $7.3\times10^6$ km$^3$ in the Bintanja scenario. Other reconstructions were calcu-

lated based on the $\delta^{18}O$ values of Bassinot et al. (1994), Lisiecki and Raymo (2005), Shackleton (2000) and Tiedemann et al. (1994). Using the LGM reconstruction of the NA and EA ice sheet volumes from Peltier (1994) as a reference for the proportionality rule leads to MIS-13.1 ice volumes ranging from 1.06 to $4.14\times10^6$ km$^3$ for EA and from 2.15 to $8.42\times10^6$ km$^3$ for NA. Corresponding sensitivity studies will be published elsewhere (Yin et al., 2007[1]) but we anticipate in saying that the conclusions reached in the present paper are qualitatively insensitive to the details of the adopted reconstruction.

For the shape of the ice sheets, we assumed that they are axi-symmetric. For a given maximum thickness, $h$, and a diameter of the circular basis at the ground, $l$, the volume of such ice sheet is

$$V = 2\pi h l^2/15$$

From there and a prescribed center, the thickness of the ice sheet at each grid point can be calculated if a relationship between $h$ and $l$ is known. As a first approximation, such relationship has been estimated from the shape and size of the ice sheets at the LGM. For NA, the diameter is about 2600 km and the altitude of its crest above the ground about 1700 m. For EA, these values are roughly 2000 km and 1480 m. These values were used in the present paper but we note that according to a theoretical model by Paterson (1994) $l$ is proportional to $h^2$, which leads to slightly different ice sheets properties. Again, these details do not qualitatively affect our conclusions (Yin et al., 2007[1]).

Finally, the locations of NA and EA were based on what we know from the initiation of the ice sheets at the last glacial inception (Clark et al., 1993; Bintanja et al., 2002; Peltier, 2004). For NA, we assumed that its center was at (90° W, 69° N) and for EA, (50° E, 63° N). Simulations were also made assuming EA is located over Scandinavia (centered at 28° E, 63° N). Although these are interesting features to be discussed in relationship with this change in location, the main conclusions remain again unchanged.

[1] Yin, Q., Berger, A., Crucifix, M., et al.: Sensitivity analyses of the size of the Eurasian ice sheet and of the Tibetan Plateau on the East Asian summer monsoon, in preparation, 2007.



## 4 Climate response of LOVECLIM at MIS-13.1

Table 2 shows the three most important results obtained from the MIS-13.1 surface temperature at the global scale and July precipitations over East China (100–120° E, 20–40° N). 506 ka BP (NH summer at perihelion, Exp. 4) is globally (annual mean and July) warmer than 495 (SH summer at perihelion, Exp. 2), a result that has been confirmed by all other experiments made where the only difference originates from the two different astronomical situations (not shown here). This underlines the major role played by the NH geographical characteristics and climatological feedbacks. Not only the Earth is globally warmer, but also the EASM is stronger when the NH summer is at perihelion. Actually there is far more precipitation over East China in July 506 ka BP (Exp. 4) than in 495 ka BP (Exp. 2) which is expected, because summer at perihelion implies enhanced seasonal contrast leading to a stronger monsoon. However, the further reinforcement of EASM precipitation in response to the introduction of ice sheets (Exp. 5) is surprising because one would normally think that the continental cooling associated with the ice sheets is unfavorable to the development of monsoon dynamics.

Figure 1a shows the precipitation anomaly resulting from the introduction of ice sheets at 506 ka BP from 80 to 150° E and from 10 to 60° N. Two main bands with increased rainfall are clearly seen. One is south of 35° N, extending from the eastern margin of the Tibetan Plateau through South China and South Japan and disappearing over the Pacific Ocean. In this belt, precipitation increases from a few percent to 30%. The other band extends from the northern margin of the Tibetan Plateau, through the northwest of China and Mongolia, and finally to the north of the Lake Baikal.

It is also significant that the pressure gradient between the ocean and the continent gets larger when the ice sheets are introduced (Fig. 1b). High geopotential over the ocean becomes larger and low geopotential deepens over land. The gradient between the ocean and the continent increases by 10–15% from the “no ice sheet” (Exp. 4) to the “with ice sheets” (Exp. 5) experiment. Consistently, we observe a reinforcement of

the easterlies blowing from the ocean to the continent, an enhanced convergence and more convective precipitation over East China. Along the coast of South-East China, the wind velocity increases by 10 to 20% and becomes definitely more easterly. At the same time, the westerly component of the wind over the continent (blowing towards the ocean) intensifies, and convergence over central China increases, which is normally expected to favour convective precipitation. In particular, the water vapor flux from the ocean to the continent is seen to increase (by 26% at 124° E–30° N for example) mainly in response to the increase in the easterly wind (from 1.6 to 2.1 $ms^{-1}$). If we analyze the water budget in the main center of precipitation increase (~118° E–30° N), we see that the precipitation change is due for 58% to the evaporation change and 42% to change in the divergence of the water vapor flux.

Although it was expected to have a reinforcement of the summer monsoon with the NH summer occurring at perihelion, it is much less evident to understand the monsoon reinforcement when the ice sheets are introduced. The global map of the difference in July precipitation between the experiment with ice sheets (Exp. 5) and the one without ice sheet (Exp. 4) (Fig. 2a) shows that, to the west of the EA ice sheet, a drier zone results from anticyclonic vorticity forced over the upslope region and to the east a wetter zone results from cyclonic vorticity forced over the downslope region. Both are expected consequences of the principle of conservation of potential vorticity. Even more significant is the appearance of a wave train propagating south-eastwards starting from the EA ice sheet and ending up over East China with a reinforcement of precipitation. This wave train corresponds to the model results of Grose and Hoskins (1979) where such a wave train is topographically induced. This wave feature is also shown in the 650-hPa-level omega field (Fig. 2b), with alternating large scale ascent and subsidence ending up with a reinforcement of the ascent over China.

This wave train is actually a robust feature of LOVECLIM. It appears also with more or less the same intensity, the same direction and the same wavelength in the following experiments:

1. other 100-yr long experiments with the same forcing and boundary conditions as



used here.

2. an experiment where the size of the EA ice sheet is doubled according to the reconstruction by Bintanja et al. (2005).
3. an experiment using a shape according to the Paterson's model assuming a perfectly plastic ice.
4. an experiment where the EA ice sheet has been moved west over Scandinavia.
5. an experiment with the same GHG concentration and ice sheets, but with NH winter at perihelion.

The phase lock which insures the reinforcement of the EASM, may be related to the Pacific Ocean, the Tibetan Plateau and/or the thermal low over East Asia. In favor of the last possibility, we find that in January (Fig. 2c), there is a wave train in the omega field like in July, but it is ending this time with a large scale subsidence which reinforces the winter thermal High over China. As far as the Tibetan Plateau is concerned, experiments have been made where it is totally removed. Comparing again the experiments with (Exp. 7) and without (Exp. 6) ice sheets in the absence of the Tibetan Plateau, the wave train is still very much present, especially in the omega field at 650 hPa level (Fig. 2d), but with a different wave length. The ascent previously centered over East China (Fig. 2b) is now over the west Pacific and is replaced by a subsidence (Fig. 2d). This leads to a largely reduced EASM, July precipitation over East China being 7% less in Exp. 7 than in Exp. 6. We can therefore conclude that the EA ice sheet reinforces the EASM over East China only through the influence of the Tibetan Plateau which is instrumental in shaping the configuration of the wave train.

Numerical experiments made for MIS-13.1 show therefore that the EASM is much stronger when NH summer is at perihelion rather than when SH summer is at perihelion, and that the EASM get reinforced again after the ice sheets are introduced. These two reinforcements lead actually to create a monsoon which is stronger at 506 ka BP than at PrI. July precipitation over East China in the experiment 506 ka BP with ice

sheets (Exp. 5) increases by about 37% when compared to the Pre-Industrial one (Table 2, Fig. 3a). At the same time, July geopotential increases over the ocean and decreases over the continent (Fig. 3b). This means that the pressure gradient between the ocean and the continent increases, leading to a 20 to 80% increase in the southwesterly and southeasterly wind velocity at the 800 hPa level over China. This leads to an increase of the water vapor flux from the ocean to the continent and to a general strengthening of the East Asian summer monsoon. Although the model simulates a situation at 506 ka BP which is globally cooler than at PrI due to the ice sheets and lower GHG concentration, NH summer at perihelion and the atmospheric wave induced by the EA ice sheet lead to a stronger monsoon than at Pre-industrial time. This strong monsoon finally contributes to increase the tree fraction over most of China, which within the resolution of the model fits well the paleo-record (not shown here).

In conclusion, the numerical experiments show that the 506 ka BP climate with ice sheets is warmer than the 495 ka BP one and has an EASM stronger than at PrI although being cooler than at this time.

## 5 Climate forcings and response at MIS-13.3

Proxy records show that the extreme monsoon over South Asia and Africa occurred near 525–530 ka BP, which is closer to MIS-13.3 than to MIS-13.1 (Bassinot et al., 1994; Rossignol-Strick et al., 1998). However, the proxy records from China show that the strong EASM occurred during the period from about 530 to 480 ka BP (e.g. Kukla et al., 1990; Guo et al., 2000). It was therefore decided to include aslo MIS-13.3 in our simulations. 524 ka BP was chosen as a compromise between the records of Lisiecki and Raymo (2005), Tiedemann et al. (1994), Bassinot et al. (1994), Shackleton (2000) and SPECMAP (Imbrie et al., 1984, provided their label 14.0 is changed into 13.3).

According to the deep-sea and ice cores, MIS-13.3 is the most glaciated and cooler peak of the whole MIS-13 interglacial. The proportionality rule used for MIS-13.1 was also used to reconstruct the ice sheets at MIS-13.3, leading to about $16.6\times10^6$ km$^3$ of



ice for the NA and EA ice sheets together, which is 50% more than at MIS-13.1. We have chosen a date of 529 ka BP for the MIS-13.3 experiment as it corresponds to the summer solstice at perihelion (we are aware that the ice volume minimum was in fact around 524 ka BP but we adopt the conservative strategy of coupling the minimum ice volume with maximum summer insolation).

The astronomical situations at 529 and 506 ka BP differ essentially through eccentricity which is much smaller at 529 ka BP (0.015 against 0.034 at 506 ka BP). This means that at 529 ka BP, the distance of the Earth to the Sun at perihelion is larger leading to less energy available in NH summer ("cooler" summer), but also to less energy globally averaged over the Earth and the year, $W$, because $W=S_0/(1-e^2)^{1/2}$ implies that $W$ is smaller for smaller values of $e$. This "cooler" NH summer at 529 ka BP leads to the continental East Asia being cooler by 1 to 2° C (not shown), but to a Pacific ocean which is not affected or is even slightly warmer. This reduces the thermal gradient between the land and the adjacent ocean leading to a weaker summer monsoon at 529 ka BP than at 506 ka BP. Consequently, July precipitation over East China is 11% less at 529 ka BP than at 506 ka BP. There is also less July precipitation over North Africa, India and East Asia.

At 529 ka BP, when the ice sheets are introduced, the same wave train as at 506 ka BP is observed in the precipitation and omega fields. Actually, all the 529 ka BP regional features are about the same as at 506 ka BP. Although weaker than at 506 ka BP, EASM at MIS-13.3 is still stronger than at PrI. July precipitation over East China at MIS-13.3 is 21% more abundant than the Pre-Industrial one and the wind velocity is 10 to 40% larger. It is therefore not surprising that the proxy data record a strong EASM during the whole MIS-13. The environment has indeed been affected already strongly by the early monsoon during MIS-13.3. This first impact has been definitely imprinted in the proxy records and reinforced later during MIS-13.13 and MIS-13.11.

## 6 Conclusions

For the first time, a set of modeling experiments have been made to understand the proxy data show an exceptionally strong East Asian summer monsoon occurring during the cool MIS-13 interglacial. The main conclusions, using the LOVECLIM model, underline the major role played by both the astronomical and the ice sheet forcings:

(1) when the Northern Hemisphere summer occurs at perihelion, like at both 529 and 506 ka BP, the East Asian summer monsoon is stronger than when Southern Hemisphere summer occurs at perihelion, like at 495 ka BP and Pre-Industrial time.

(2) the Eurasian ice sheet (its albedo and topography which was deduced from the $\delta^{18}O$ record) further enhances the East Asian summer monsoon through a wave train propagating southeastwards from the Eurasian ice sheet. This wave train ending with a large scale ascent over East China is influenced by the Tibetan Plateau and probably phase locked by the East Asian summer low. A consistent pattern of responses is then observed, made of an increase of the air pressure gradient between the Pacific Ocean and the East Asian continent, an intensification of the low-level southeasterlies blowing from the ocean and an enhanced precipitation over East China.

These are preliminary results which must be confirmed by other more sophisticated climate models and by further sensitivity analyses to the volume and location of the ice sheets and to the size of the Tibetan Plateau.

*Acknowledgements.* Q. Z. Yin has benefited from a grant of the Belgium FNRS (Fonds de la Recherche Scientifique) and is now postdoctoral fellow at Université catholique de Louvain in Louvain-la-Neuve. M. Crucifix and H. Goosse are research associates with the FNRS.



## References

Bassinot, F. C., Labeyrie, L. D., Vincent, E., Quidelleur, X., Shackleton, N. J., and Lancelot, Y.: The astronomical theory of climate and the age of the Brunhes-Matuyama magnetic reversal, Earth Planet. Sc. Lett., 126, 91–108, 1994.

Berger, A.: Long-term variations of daily insolation and Quaternary Climatic Changes, J. Atmos. Sci., 35(12), 2362–2367, 1978.

Bintanja, R., van de Wal, R. S. W., and Oerlemans, J.: Modelled atmospheric temperatures and global sea level over the past million years, Nature, 437, 125–128, 2005.

Bintanja, R., van de Wal, R. S. W., and Oerlemans, J.: Global ice volume variations through the last glacial cycle simulated by a 3-D ice-dynamical model, Quatern. Int., 95–96, 11–23, 2002.

Braconnot, P., Otto-Bliesner, B., Harrison, S., Joussaume, S., Peterschmitt, J.-Y., Abe-Ouchi, A., Crucifix, M., Driesschaert, E., Fichefet, T., Hewitt, C. D., Kageyama, M., Kitoh, A., Laîné, A., Loutre, M.-F., Marti, O., Merkel, U., Ramstein, G., Valdes, P., Weber, S. L., Yu, Y., and Zhao, Y.: Results of PMIP2 coupled simulations of the Mid-Holocene and Last Glacial Maximum – Part 1: experiments and large-scale features, Clim. Past, 3, 261–277, 2007, http://www.clim-past.net/3/261/2007/.

Brovkin, V., Ganapolski, A., and Svirezhev, Y.: A continuous climate-vegetation classification for use in climate-biosphere studies, Ecol. Modell., 101, 251–261, 1997.

Chen, F. H., Bloemendal, J., Zhang, P. Z., and Liu, G. X.: An 800 ky proxy record of climate from lake sediments of the Zoige Basin, eastern Tibetan Plateau, Palaeogeography, Palaeoclimatology, Palaeoecology, 151, 307–320, 1999.

Clark, P. U. and Mix, A. C. (Eds.): Ice sheets and sea level of the last glacial maximum, Quaternary Sci. Rev., 21(1–3), 2002.

Clark, P. U., Clague, J. J., Curry, B. B., Dreimanis, A., Hicock, S. R., Miller, G. H., Berger, G. W., Eyles, N., Lamothe, M., Miller, B. B., Mott, R. J., Oldale, R. N., Stea, R. R., Szabo, J. P., Thorleifson, L. H., and Vincent, J.-S.: Initiation andd evelopment of the Laurentide and Cordilleran ice sheets following the last interglaciation, Quaternary Sci. Rev., 12, 79–114, 1993.

Driesschaert, E., Fichefet, T., Goosse, H., Huybrechts, P., Janssens, I., Mouchet, A., Munhoven, G., Brovkin, V., and Weber, S. L.: Modeling the influence of Greenland ice sheet melting on the Atlantic meridional overturning circulation during the next millennia, Geophys.

Res. Lett., 34, L10707, doi:10.1029/2007GL029516, 2007.
Duplessy, J. C., D. M., and Kageyama, M.: The Deep Ocean During the Last Interglacial Period, Science, 316, 89–91, 2007.
EPICA community members: Eight glacial cycles from an Antarctic ice core, Nature, 429, 623–628, 2004.
Gingele, F. X. and Schmieder, F.: Anomalous South Atlantic lithologies confirm global scale of unusual mid-Pleistocene climate excursion, Earth Planet. Sc. Lett., 186, 93–101, 2001.
Goosse H. and Fichefet, T.: Importance of ice-ocean interactions for the global ocean circulation: a model study, J. Geophys. Res., 104(C10), 23 337–23 355, 1999.
Grose, W. L. and Hoskins, B. J.: On the Influence of Orography on Large-Scale Atmospheric Flow, J. Atmos. Sci., 36, 223–234, 1979.
Guo, Z. T., Biscaye, P., Wei, L. Y., Chen, X. F., Peng, S. Z. and Liu, T. S.: Summer monsoon variations over the last 1.2 Ma from the weathering of loess-soil sequences in China, Geophys. Res. Lett., 27, 1751–1754, 2000.
Harris, S. E. and Mix, A. C.: Pleistocene precipitation Balance in the Amazon Basin recorded in deep sea sediments, Quaternary Res., 51, 14–26, 1999.
Hughes, T. J., Denton, G. H., Andersen, B. G., Schilling, D. H., Fastook, J. L., and Lingle, C. S.: The last great ice sheets: A global view, in: The last great ice sheets, edited by: Denton, G. H. and Hughes, T. J., J. Wiley & Sons, New York, 263–317, 1981.
Imbrie, J., Berger, A., Boyle, E. A., Clemens, S. C., Duffy, A., Howard, W. R., Kukla, G., Kutzbach, J., Martinson, D. G., McIntyre, A., Mix, A. C., Molfino, B., Morley, J. J., Peterson, L. C., Pisias, N. G., Prell, W. L., Raymo, M. E., Shackleton, N. J., and Toggweiler, J. R.: On the structure and origin of major glaciation cycles, 2. The 100 000-year cycle, Paleoceanography, 8(6), 699–735, 1993.
Imbrie, J., Hays, J. D., Martinson, D. G., McIntyre, A., Mix, A. C., Morley, J. J., Pisias, N. G., Prell, W. L., and Shackleton, N. J.: The orbital theory of Pleistocene climate: support from a revised chronology of the marine $\delta^{18}$O record, in: Milankovitch and Climate, Part 1, edited by: Berger, A. L., Imbrie, J., Hays, J., et al., D. Reidel Pub. Co., 269–305, 1984.
Jouzel, J., Masson-Delmotte, V., Cattani, O., Dreyfus, G., Falourd, S., Hoffmann, G., Minster, B., Nouet, J., Barnola, J. M., Chappellaz, J., Fischer, H., Gallet, J. C., Johnsen, S., Leuenberger, M., Loulergue, L., Luethi, D., Oerter, H., Parrenin, F., Raisbeck, G., Raynaud, D., Schilt, A., Schwander, J., Selmo, E., Souchez, R., Spahni, R., Stauffer, B., Steffensen, J. P., Stenni, B., Stocker, T. F., Tison, J. L., Werner, M., and Wolff, E. W.: Orbital and Millennial Antarctic



Climate Variability over the Past 800 000 Years, Science, 317, 793–796, 2007.
Kukla, G., An, Z. S., Melice, J. L., Gavin, J., and Xiao, J. L.: Magnetic susceptibility record of Chinese Loess, Trans. R. Soc. Edinb. Earth sci., 81, 263–288, 1990.
Lambeck, K., Esat, T. M., and Potter, E. K.: Links between climate and sea levels for the past three million years, Nature, 419, 199–206, 2002.
Lisiecki, L. E. and Raymo, M. E.: A Pliocene-Pleistocene stack of 57 globally distributed benthic delta $\delta^{18}$O records, Paleoceanography, 20(1), PA1003; doi:10.1029/2004PA001071, 2005.
Opsteegh, J. D., Haarsma, R. J., Selten, F. M., and Kattenberg, A.: ECBILT: A dynamic alternative to mixed boundary conditions in ocean models, Tellus, 50A, 348–367, 1998.
Paterson, W. S. B.: The Physics of Glaciers, Pergamon, Tarrytown, N.Y., 480 pp., 1994.
Peltier, W. R.: "Implicit ice" in the global theory of glacial isostatic adjustment, Geophys. Res. Lett., 25(21), 3955–3958, 1998.
Peltier, W. R.: Ice age paleotopography, Science, 265, 195–201, 1994.
Peltier, W. R.: Global glacial isostasy and the surface of the ice-age Earth: the ICE-5G (VM2) model and GRACE, Ann. Rev. Earth Planet Sci., 32, 111–149, 2004.
Prokopenko, A. A., Williams, D. F., Kuzmin, M. L., Karabanov, E. B., Khursevich, G. and Peck, J. A.: Muted climate variations in continental Siberia during the mid-Pleistocene epoch, Nature, 418, 65–68, 2002.
Rossignol-Strick, M., Paterne, M., Bassinot, F. C., Emeis, K.-C., and De Lange, G. J.: An unusual mid-Pleistocene monsoon period over Africa and Asia, Nature, 392, 269–272, 1998.
Shackleton, N. J.: The 100 000-year Ice-Age Cycle identified and found to lag temperature, carbon dioxide and orbital eccentricity, Science, 289, 1897–1902, 2000.
Siegenthaler, U., Stocker, T. F., Monnin, E., L¨uthi, D., Schwander, J., Stauffer, B., Raynaud, D., Barnola, J.-M., Ficher, H., Masson-Delmott, V., and Jouzel, J.: Stable carbon cycle-climate relationship during the late Pleistocene, Science, 310, 1313–1317, 2005.
Spahni, R., Chappellaz, J., Stocker, T. F., Loulergue, L., Hausammann, G., Kawamura, K., Fluckiger, J., Schwander, J., Raynaud, D., Masson-Delmotte, V., and Jouzel, J.: Atmospheric Methane and Nitrous Oxide of the Late Pleistocene from Antarctic Ice Cores, Science, 310, 1317–1321, 2005.
Tiedemann, R., Sarntheim, M., and Shackleton, N. J.: Astronomic timescale for the Pliocene Atlantic $\delta^{18}$O and dust flux records of Ocean Drilling Program site 659, Paleoceanography, 9, 619–638, 1994.
Timmermann, A., Justino Barbosa, F., Jin, F. F., and Goosse, H.: Surface temperature control

in the North Pacific during the last glacial maximum, Clim. Dyn., 23, 353–370, 2004.
Wang, P., Tian, J., Cheng, X., Liu, C., and Xu, J.: Major Pleistocene stages in a carbon perspective: The South China Sea record and its global comparison, Paleoceanography, 19, PA4005, doi:10.1029/2003PA000991, 2004.
Yin, Q. Z. and Guo, Z. T.: Mid-Pleistocene vermiculated red soils in southern China as an indication of unusually strengthened East Asian monsoon, Chinese Science Bulletin, 51(2), 213–220, 2006.
Yin, Q. Z. and Guo, Z. T.: Strong summer monsoon during the cool MIS-13, Clim. Past Discuss., 3, 1119–1132, 2007, http://www.clim-past-discuss.net/3/1119/2007/.



**Table 1.** The forcings for the different simulations.

| Experiments No. | Time (ka BP) | $CO_2$ (ppmv) | $CH_4$ (ppbv) | $N_2O$ (ppbv) | Eccentricity | Obliquity (°) | Longitude of Perihelion (°) | Ice sheets | Tibetan Plateau |
|---|---|---|---|---|---|---|---|---|---|
| Exp. 1 | 0 | 280 | 760 | 270 | 0.016724 | 23.446 | 102.04 | No | Yes |
| Exp. 2 | 495 | 240 | 510 | 280 | 0.038638 | 23.903 | 97.82 | No | Yes |
| Exp. 3 | 495 | 240 | 510 | 280 | 0.038638 | 23.903 | 97.82 | Yes | Yes |
| Exp. 4 | 506 | 240 | 510 | 280 | 0.034046 | 23.377 | 274.05 | No | Yes |
| Exp. 5 | 506 | 240 | 510 | 280 | 0.034046 | 23.377 | 274.05 | Yes | Yes |
| Exp. 6 | 506 | 240 | 510 | 280 | 0.034046 | 23.377 | 274.05 | No | No |
| Exp. 7 | 506 | 240 | 510 | 280 | 0.034046 | 23.377 | 274.05 | Yes | No |
| Exp. 8 | 529 | 240 | 530 | 280 | 0.015078 | 23.622 | 268.25 | No | Yes |
| Exp. 9 | 529 | 240 | 530 | 280 | 0.015078 | 23.622 | 268.25 | Yes | Yes |

Astronomical parameters are from Berger (1978). For GHG: (1) 0 ka BP is for Pre-Industrial time. The values are used in the Paleoclimate Modeling Intercomparison Project (Braconnot et al., 2007). (2) The values for 495 and 506 ka BP are kinds of averages for the whole MIS-13.1 to allow using the same values for the two experiments. They are based upon EPICA (2004), Siegenthaler et al. (2005) and Spahni et al. (2005), but taking into account the new time scale of Jouzel et al. (2007). (3) The values for 529 ka BP are also estimated using EPICA but taking into account the new time scale of Jouzel et al. (2007). Ice sheets means North American and Eurasian ice sheets. The experiments are 2000-year long simulations and the climate averages are computed over the last 100 years

**Table 2.** Surface temperature for the whole Earth and precipitation over East China for the 495, 506 and 529 ka BP experiments. All the values are relative to the simulated Pre-Industrial ones.

| Experiments | Global Surface temperature (°C) | | | Precipitation over East China (%) | | |
|---|---|---|---|---|---|---|
| | January | July | Annual | January | July | Annual |
| Exp. 2 | −0.08 | −0.99 | −0.41 | 0 | −16 | −5 |
| Exp. 4 | −1.07 | 0.84 | −0.18 | −5 | 32 | 7 |
| Exp. 5 | −1.7 | 0.58 | −0.64 | −15 | 37 | 2 |
| Exp. 8 | −0.75 | 0.46 | −0.18 | −5 | 18 | 4 |
| Exp. 9 | −1.47 | 0.04 | −0.75 | −10 | 21 | −4 |



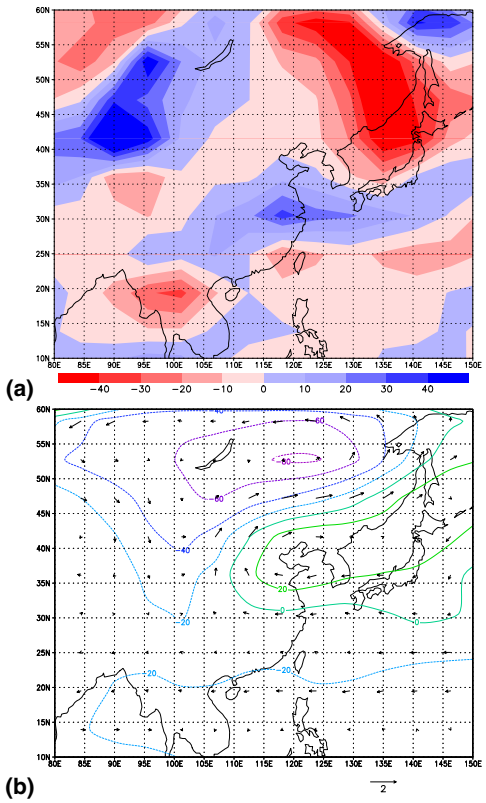


**Fig. 1.** Exp. 5 minus Exp. 4 for **(a)** July precipitation (cm/year) and **(b)** July geopotential ($m^2\ S^{-2}$) and wind (m/s) at 800 hPa level.

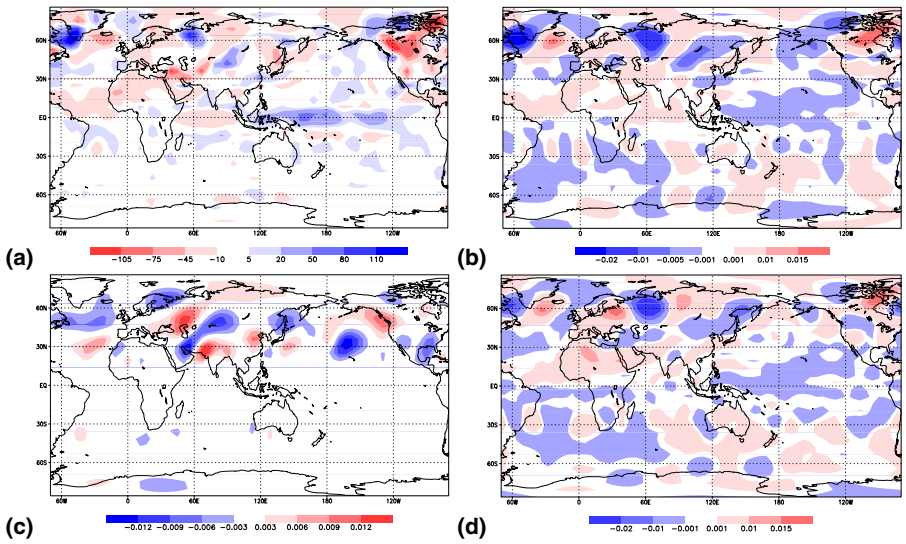


**Fig. 2.** **(a)** July precipitation (cm/year), **(b)** July 650-hPa-level omega field (Pa/s) and **(c)** January 650-hPa-level omega field (Pa/s) for Exp. 5 minus Exp. 4. **(d)** July 650-hPa-level omega field (Pa/s) for Exp. 7 minus Exp. 6. Fig. 2d has been placed here to allow any easy comparison with Fig. 2b.



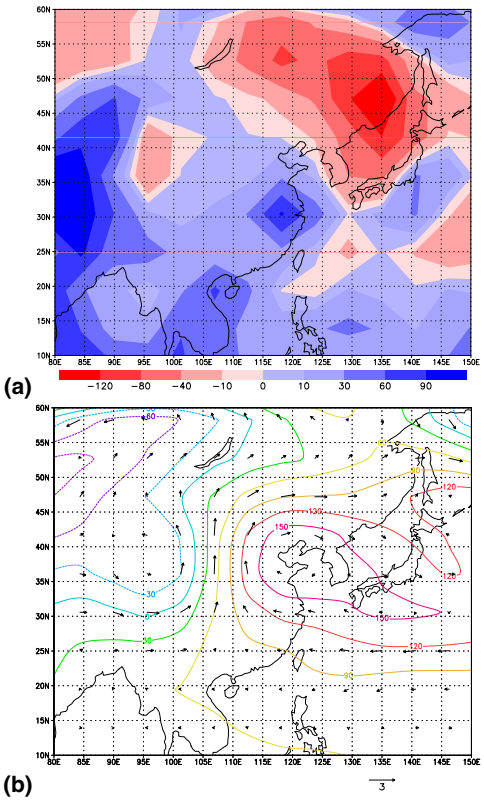


**Fig. 3.** Exp. 5 minus Exp. 1 for **(a)** July precipitation (cm/year) and **(b)** July geopotential ($m^2\ S^{-2}$) and wind (m/s) at 800 hPa level.